

Instability of $\text{Pa}\bar{3} \text{Cs}_3\text{C}_{60}$ at ambient pressure and superconducting state of the FCC phase

Changming Yue,^{1,*} Yusuke Nomura,² Kosmas Prassides,³ and Philipp Werner^{1,†}

¹*Department of Physics, University of Fribourg, 1700 Fribourg, Switzerland*

²*Department of Applied Physics and Physico-Informatics, Keio University, 3-14-1 Hiyoshi, Kohoku-ku, Yokohama, 223-8522, Japan*

³*Department of Physics, Graduate School of Science, Osaka Metropolitan University, Osaka 599-8531, Japan*

The alkali-doped fulleride Cs_3C_{60} , crystallized in the space group $\text{Fm}\bar{3}\text{m}$ or $\text{Pm}\bar{3}\text{n}$, exhibits unconventional s -wave superconductivity under pressure with a maximum $T_c \sim 38$ K. Recently, a new primitive-cubic-structured Cs_3C_{60} phase corresponding to the space group $\text{Pa}\bar{3}$ has been reported (arXiv:2208.09429) and the authors observed superconductivity at ambient pressure. Using density-functional theory (DFT) calculations, we show that the proposed $\text{Pa}\bar{3}$ structure is not stable under ionic relaxation, but transforms into the FCC structure. We study the normal and superconducting state of the stable FCC phase at different temperatures and volumes using DFT plus dynamical mean-field theory (DFT+DMFT) in the Nambu formalism. As temperature increases, the transition between superconductor and normal metal (Mott insulator) at small (big) volume is found to be second (first) order. The recently developed maximum entropy analytic continuation method for the anomalous-self-energy is used to study the momentum-resolved spectra and optical conductivity.

Introduction. The trivalent alkali-doped fullerenes A_3C_{60} ($A = \text{K}, \text{Rb}$) are fullerene-based molecular superconductors at ambient pressure, while the volume expanded Cs_3C_{60} with larger cation size becomes superconducting upon application of pressure [1, 2]. Cs_3C_{60} is known to exist in two types of crystal structures, the FCC (A15) structure with the space group $\text{Fm}\bar{3}\text{m}$ ($\text{Pm}\bar{3}\text{n}$), where the C_{60} molecules are arranged on a face (body) centered cubic [FCC (BCC)] lattice. Both FCC and A15 Cs_3C_{60} are Mott insulators at ambient pressure. The highest T_c in A_3C_{60} is realized in A15 Cs_3C_{60} at a pressure of ~ 0.7 GPa ($T_c \sim 38$ K), while the highest T_c in FCC Cs_3C_{60} is 35 K at the same pressure [3–5]. For both structures, the phase diagram in the space of temperature and pressure (or inverse volume per C_{60}) exhibits an s -wave superconducting state with a dome-shaped T_c next to an antiferromagnetic or paramagnetic Mott insulator (Néel temperature $T_N \sim 46$ K for A15 and 2.2 K for FCC) [4–6], which suggests an unconventional pairing mechanism in A_3C_{60} [2, 4, 7, 8]. A_3C_{60} is a strongly correlated three-orbital electron system, where the bandwidth W of the t_{1u} bands ranges from 0.3 to 0.5 eV and the on-molecule intra-orbital interaction U ranges from 0.8 to 1.1 eV, depending on the type of alkali metal and the volume per C_{60} [9]. The electron-phonon coupling between the extended t_{1u} molecular orbitals and the intramolecular Jahn-Teller H_g phonon modes results in unusual multiorbital interactions, with an effectively negative (antiferromagnetic) Hund coupling J_{eff} [8, 10]. As a result, the system exhibits a reversed Hund’s rule, which favors low spin and angular momentum states. The negative J_{eff} and strong on-molecule Coulomb interactions are

at the origin of the various unconventional normal phases realized in A_3C_{60} , including the Jahn-Teller metal [6, 11] and the s -wave superconducting state [2, 11]. The pairing glue in this $J_{\text{eff}} < 0$ system is provided by enhanced local orbital fluctuations [11]. In the superconducting phase, these fluctuations are proportional to the pairing strength and peak in the strongly correlated metal regime [12]. Superconductivity in fullerenes is thus conceptually linked to the spin-freezing induced unconventional superconductivity in positive- J systems like uranium and iron-based superconductors [13] and even cuprates [14].

For experiments and practical applications, it is desirable to realize superconductivity at ambient pressure. A recent preprint reported superconductivity with $T_c \sim 22$ K in a Cs_3C_{60} sample at ambient pressure [15]. According to this study, the newly discovered phase has a primitive cubic structure with the space group $\text{Pa}\bar{3}$, and features a particular type of orientational order of the molecules. Remarkably, the reported evolution of T_c in $\text{Pa}\bar{3} \text{Cs}_3\text{C}_{60}$ under pressure as a function of volume per C_{60} extends to very small volumes ($V = 660 \sim 700 \text{ \AA}^3$), which has not been reported before in the FCC and A15 Cs_3C_{60} systems [4]. The trend for very small volumes follows closely that of K_3C_{60} under pressure [16].

Motivated by the findings in Ref. 15, we investigate the electronic structure and lattice properties of $\text{Pa}\bar{3} \text{Cs}_3\text{C}_{60}$. Our simulations based on density functional theory (DFT) show that $\text{Pa}\bar{3} \text{Cs}_3\text{C}_{60}$ at the reported unit cell volume is unstable and relaxes to the FCC structure. We thus study the normal and superconducting states of the stable FCC structure for different volumes, but do not find superconductivity for $V \lesssim 700 \text{ \AA}^3$. At higher volumes our simulations yield a superconducting phase with T_c values close to those reported in previous experiments on Cs_3C_{60} under pressure. Also the computed optical conductivity data are consistent with previous optical experiments.

* changming.yue@unifr.ch

† philipp.werner@unifr.ch

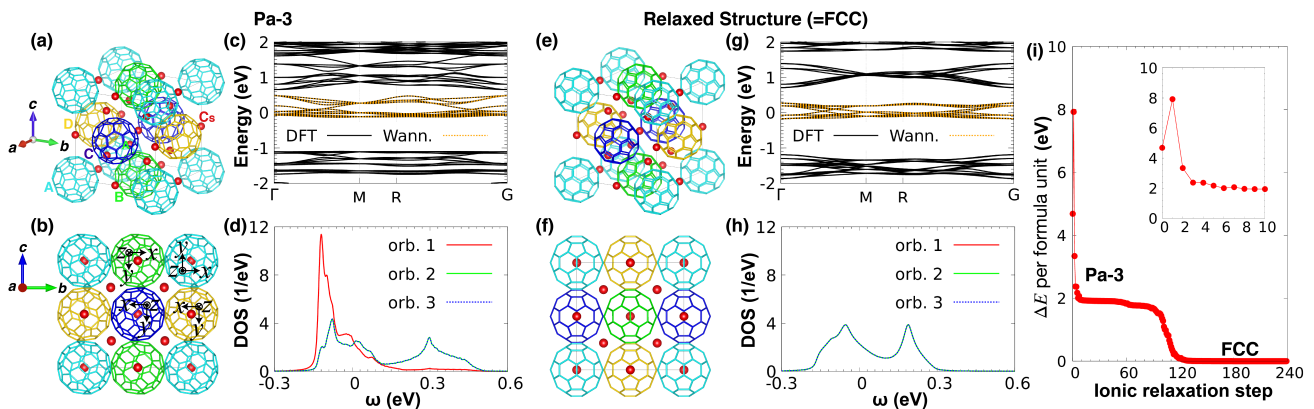


FIG. 1. Crystal structure and electronic structure of Cs_3C_{60} . (a-b) [(e-f)] Oblique and side view of the $\text{Pa}\bar{3}$ [relaxed (FCC)] crystal structure. The red spheres show the Cs atoms with an exaggeratedly small radius. The $\text{Pa}\bar{3}$ structure, whose primitive cell is the same as the unit cell, contains four C_{60} molecules, with different local coordinates each. For a better visualization, molecule A centered at $(0.0, 0.0, 0.0)$ is colored in cyan, B at $(0.5, 0.5, 0.0)$ in green, C at $(0.0, 0.5, 0.5)$ in blue, and D at $(0.5, 0.0, 0.5)$ in gold. The black arrows in panel (b) illustrate the local xyz -coordinate system for each molecule. The DFT (black) bands and their Wannier interpolations (orange) are shown in panel (c) for the $\text{Pa}\bar{3}$ structure and in panel (g) for the relaxed structure. Panels (d) and (h) show the corresponding relaxed structure on-molecule orbital-resolved DOS per spin, which are the same for all molecules, since they have the same environment relative to the local xyz -coordinate system. (i) The energy difference ΔE per C_{60} between the structure under relaxation and the final stable FCC structure as a function of ionic relaxation steps. The initial structure is the experimental $\text{Pa}\bar{3}$ structure, whose energy per formula unit is 4.67 eV higher than in the final stable FCC structure. The inset shows a zoom of the initial 11 steps.

Unstable $\text{Pa}\bar{3}$ crystal structure. The $\text{Pa}\bar{3}$ Cs_3C_{60} crystal structure proposed in Ref. 15 is shown in Fig. 1(a,b). In the unit-cell, there are four C_{60} molecules which are orientationally ordered in essentially the same way as in the pure C_{60} crystal [18]. The $\text{Pa}\bar{3}$ structure can be constructed from the orientationally ordered FCC one [19] by rotating the four C_{60} molecules clockwise by the same angle ϕ ($\approx 22^\circ$), but about different local $\langle 111 \rangle$ axes [18]. The Cs atoms (red spheres) are located at the octahedral and tetrahedral holes formed by the close-packed stacking of the C_{60} molecules along the $[111]$ crystal direction. In the local coordinates $\{x, y, z\}$, the four molecules are equivalent to each other, as shown in Fig. 1(b).

Our analysis suggests that the $\text{Pa}\bar{3}$ structure reported in Ref. 15 is not stable. The Cs atoms are easily ionized and donate an electron each to the fullerene molecules. The ionic radius of Cs^+ is $r_{\text{Cs}^+} = 1.67 \text{ \AA}$ and the van der Waals radius of C is $r_{\text{vdW,C}} = 1.7 \text{ \AA}$. However, according to the experimental structure, the nearest Cs^+ -C distance for the Cs^+ located in the tetrahedral hole is 2.7 \AA , which is much smaller than $\sim r_{\text{Cs}^+} + r_{\text{vdW,C}} = 3.37 \text{ \AA}$. Such a small Cs-C distance would require a significant external pressure and hence the proposed structure cannot be stable at ambient pressure. $\text{Pa}\bar{3}$ fullerides have been studied for several decades, for example $\text{Na}_2\text{CsC}_{60}$ [17] which is superconducting at ambient pressure with $T_c = 12 \text{ K}$. In $\text{Na}_2\text{CsC}_{60}$, the distance between the tetrahedral Na^+ and nearest C is 2.96 \AA , which is bigger than $r_{\text{Na}^+} + r_{\text{vdW,C}} = 0.95 + 1.7 = 2.65 \text{ \AA}$ [see Supplementary Material (SM.1)]. If however the tetrahedral sites incorporate K, Rb or Cs, or any atoms with a size larger than the size of the hole, these simple geometrical considera-

tions essentially exclude the existence of such a structure.

We confirmed the structural instability of $\text{Pa}\bar{3}$ Cs_3C_{60} at the reported volume by performing a crystal structure relaxation at fixed volume, using the Vienna ab initio simulation package (VASP) [20, 21, 23] (SM. 2). Figure 1(i) shows the evolution of the energy difference ΔE per formula unit between the structure under relaxation and the final stable FCC structure. We start from the experimentally determined $\text{Pa}\bar{3}$ structure [15], which turns out to have a much higher energy than the FCC structure, with $\Delta E \approx 4.67 \text{ eV}$. This indicates that the $\text{Pa}\bar{3}$ structure is energetically unstable. The structural relaxation is accompanied by rotations of the C_{60} molecules and the alignment of the local coordinate systems (see SM. 2). The distance between the tetrahedral Cs^+ and its nearest C in the relaxed FCC structure is 3.25 \AA , which is still smaller than $r_{\text{Cs}^+} + r_{\text{vdW,C}} = 3.37 \text{ \AA}$ and corresponds to a significant pressure of approximately 2.2 GPa at $T = 15.4 \text{ K}$ [22] (or an even higher pressure at room temperature). We note, however, that these results for $\text{Cs}_3\text{Cs}_{60}$ do not imply that all $\text{Pa}\bar{3}$ structures are unstable. The $\text{Pa}\bar{3}$ $\text{Na}_2\text{CsC}_{60}$ structure reported in Ref. 17 is stable against relaxation, consistent with the above-mentioned fact that Na^+ fits well into the tetrahedral hole (see SM.2).

Large crystal field splitting in the $\text{Pa}\bar{3}$ structure. The band structure (black lines) of the unstable $\text{Pa}\bar{3}$ structure is shown in Fig. 1(c). The tight-binding (TB) Hamiltonian for the bands near the Fermi energy is obtained from the maximally-localized Wannier functions constructed by wannier90 [24, 25]. These TB bands (orange lines) reproduce the low-energy DFT bands very well. We choose

orbitals which diagonalize the onsite Hamiltonian of each C_{60} molecule. As the four molecules in the unit cell are equivalent to each other in the local coordinates, the density of states (DOS) and crystal field (CF) splittings are the same. As shown in Fig. 1(d), the 3-fold degenerate t_{1u} orbitals of the isolated molecule are split in a “one down, two up” fashion, with orbital 1 lying below the degenerate orbitals 2 and 3. According to the on-molecule Hamiltonian of the Wannier TB model, the CF splitting in the Pa $\bar{3}$ structure is as big as 164 meV. The FCC structure instead has no CF splitting, as shown by the triply degenerate DOS in Fig. 1(h). CF splittings in fullerenes tend to suppress superconductivity [26, 27] since they reduce the local orbital fluctuations and hence weaken the pairing glue [28].

Ab-initio calculations. The realistic effective on-molecule Coulomb interactions U_{eff} and Hund couplings J_{eff} are shown in the fifth and sixth rows of Tab. I. They are derived by considering two contributions. The first contribution, $U(J)_{\text{cRPA}}$, is the static interaction obtained by the constrained random phase approximation (cRPA) [29], which considers the screening by electrons in higher-energy bands. The second contribution, $U(J)_{\text{ph}}$, is due to phonon screening and is obtained within constrained density functional perturbation theory [30]. We calculated $U(J)_{\text{cRPA}}$ for the different volumes using the VASP code [20, 21, 23] and report the values in the first and second rows of Tab. I. The parameters $U(J)_{\text{ph}}$ were obtained by linear extrapolation of the data presented in Ref. 30 and are listed in the third and fourth rows of Tab. I. The bandwidth W of the TB bands is shown in the 7th row. J_{eff} is negative for all volumes, which shows that the Hund coupling is inverted due to the overscreening by the phonons.

We solve the realistic three-band Hubbard model for the t_{1u} orbitals with rotationally invariant Kanamori interactions in the framework of DFT plus dynamical

TABLE I. Volume dependence of the orbital average of the static on-site interaction parameters and bandwidth for FCC Cs_3C_{60} . The first and second row show the static Coulomb interaction U_{cRPA} and the exchange interaction J_{cRPA} calculated by cRPA. The third and fourth row show the phonon-mediated static Coulomb interactions U_{ph} and on-site exchange interaction J_{ph} extracted from Ref. 30. The fifth and sixth row show the effective interaction $U(J)_{\text{eff}} = U(J)_{\text{cRPA}} + U(J)_{\text{ph}}$. The last row shows the bandwidth W of the target bands. The energies are in eV.

V (\AA^3)	675	700	724.8	750	775
U_{cRPA}	0.6286	0.7462	0.8269	0.8872	0.9814
J_{cRPA}	0.0417	0.0354	0.0367	0.0372	0.0386
U_{ph}	-0.17	-0.16	-0.1479	-0.142	-0.120
J_{ph}	-0.05	-0.05	-0.05	-0.05	-0.051
U_{eff}	0.5686	0.5862	0.6790	0.7452	0.8614
J_{eff}	-0.0083	-0.0146	-0.0133	-0.0128	-0.0124
W	0.570	0.528	0.474	0.429	0.367
T_c (K)	<7.5	<7.5	17.7	33.7	42.5

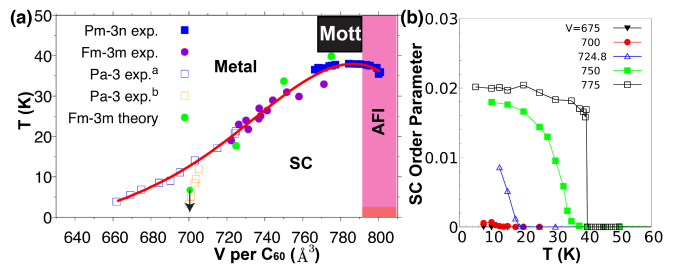


FIG. 2. (a) Superconducting phase of Cs_3C_{60} as a function of volume per C_{60} . The green circles show the T_c of the FCC structure obtained using DFT+DMFT in the Nambu formalism. The blue empty squares (with superscript a) and red solid line show the T_c of the Pa $\bar{3}$ structure reported in Ref. 15. The pink (orange) shading indicates the antiferromagnetic insulator phase for Pm $\bar{3}n$ (Fm $\bar{3}m$) with Néel temperature $T_N \sim 46$ (2.2) K. The light orange empty squares (with superscript b) mark the T_c for $Na_2Rb_xCs_{1-x}C_{60}$ in the Pa $\bar{3}$ structure [39, 40]. The solid squares and dots show the T_c for the A15 and FCC structure reproduced from Refs. [4, 41, 42], respectively. The black region schematically indicates the Mott insulating solutions at elevated temperature above T_c near $V = 775 \text{ \AA}^3$. (b) The T -dependence of the superconducting order parameter for FCC Cs_3C_{60} for the indicated volumes in the FCC structure.

mean-field theory (DMFT) [31, 32]. To deal with the s -wave intra-orbital spin-singlet pairing, we implement DFT+DMFT in the Nambu formalism and solve the corresponding three-orbital Anderson impurity model with a superconducting bath using continuous-time quantum Monte Carlo simulations based on the hybridization expansion (CT-HYB) [33, 34]. Four-operator updates are implemented to ensure the ergodicity of the Monte Carlo sampling in the symmetry-broken phase [35]. Furthermore, the worm algorithm is used to measure the Green’s function [36–38]. The calculations are constrained to paramagnetic and orbitally symmetrized solutions.

Superconductivity in the stable FCC structure. Since the Pa $\bar{3}$ structure is unstable, we instead study the superconducting and normal states of FCC Cs_3C_{60} under pressure (for compressed volumes). Figure 2(a) shows the calculated T_c which is determined from the temperature dependence of the superconducting order parameter as shown in Fig. 2(b). Our results for T_c well reproduce the experimental T_c for the FCC structure obtained by Ganin *et al.* [4] in the volume range $V \sim 720 - 780 \text{ \AA}^3$. For $V \leq 700 \text{ \AA}^3$, no signature of superconductivity is found at the lowest temperature (~ 7.5 K) we can reach in the DFT+DMFT calculations. The trend of the calculated T_c with decreasing volume is not consistent with the trend reported in Ref. 15 (red solid line) for the Pa $\bar{3}$ structure. On the small volume side, the $T_c < 7.5$ K for $V \sim 700 \text{ \AA}^3$ is instead similar to that of $Na_2Rb_xCs_{1-x}C_{60}$ in the Pa $\bar{3}$ structure reported in Ref. 39. The red solid line at $V < 700 \text{ \AA}^3$ roughly matches the results for K_3C_{60} under pressure [39].

A noteworthy observation is that the transition from

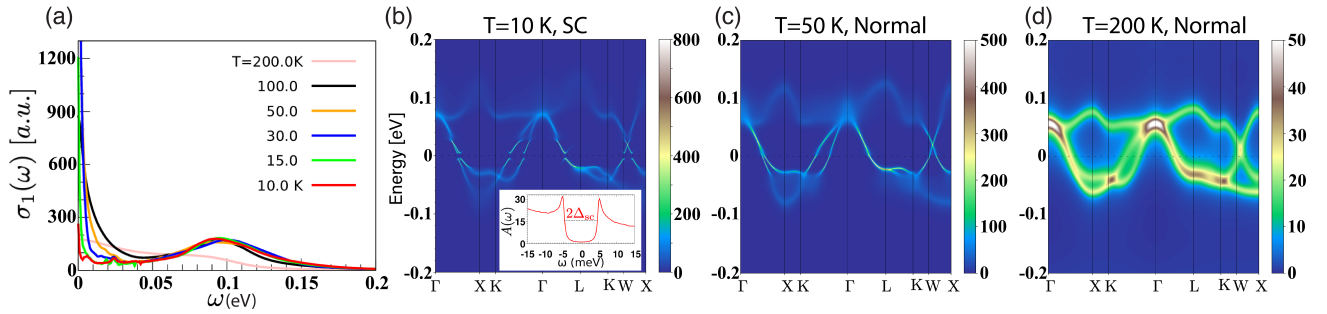


FIG. 3. Optical conductivity $\sigma_1(\omega)$ (a) and momentum-resolved spectral function $A(\mathbf{k}, \omega)$ (b-d) in a narrow energy window $-0.2 < \omega < 0.2$ eV at $V = 750 \text{ \AA}^3$ at the indicated temperatures. The inset in panel (b) shows the low-energy \mathbf{k} -integrated normal spectrum $A(\omega)$ with Δ_{sc} the SC gap.

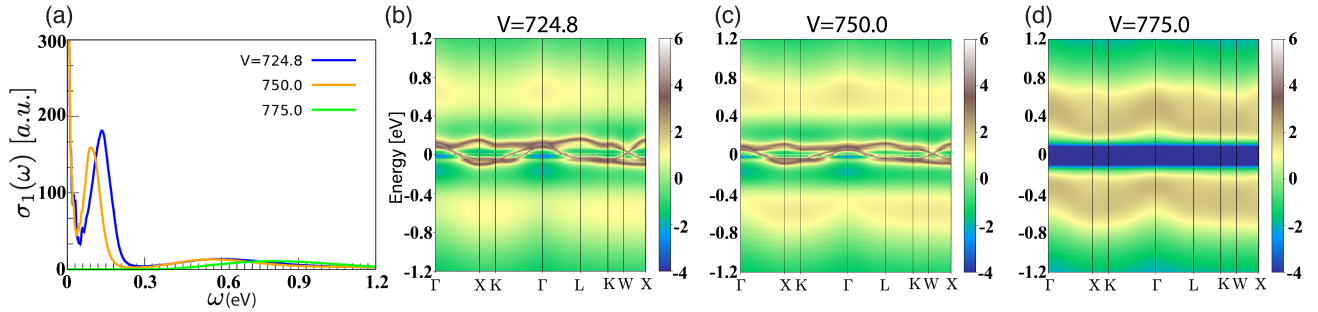


FIG. 4. Optical conductivity (a) and momentum-resolved spectral function $A(\mathbf{k}, \omega)$ (b-d) in a wide energy window $-1.2 < \omega < 1.2$ eV, for the normal state at $T = 50 (> T_c)$. The volumes are indicated in each panel. In (b-d), we show the intensity on a log scale for a better visualization of the Hubbard bands.

the s -wave unconventional superconductor to the metallic state is second order, while the transition to the Mott insulator is discontinuous. This can be seen from $\Delta(T)$, the temperature dependence of the superconducting order parameter. At $V = 750 \text{ \AA}^3$, where the system is moderately correlated, $\Delta(T)$ follows the relation $\Delta(T) \propto |T - T_c|^{1/2}$ near the critical point, and we use this relation to determine T_c . At $V = 775 \text{ \AA}^3$, in the strong correlation regime, $\Delta(T)$ drops abruptly to 0 as the system enters the Mott insulating phase. The first order transition from superconductor to Mott insulator seen in Cs_3C_{60} on the strong coupling side of the dome is similar to that between the d -wave superconductor and Mott insulator reported in Refs. 43 and 44.

Momentum-resolved spectra and optical conductivity. The momentum-resolved spectrum can be calculated from the Green's function G as $A(\mathbf{k}, \omega) = -2 \sum_{\alpha=1}^3 \text{Im} G_{\alpha\uparrow, \alpha\uparrow}(\mathbf{k}, \omega) / \pi$, where the factor of 2 comes from the spin degeneracy. In the superconducting state, to get the real frequency lattice Green's function $G(\mathbf{k}, \omega)$, one has to perform an analytic continuation from the Matsubara to the real frequency axis not only of the normal self-energy Σ^{nor} , but also of the anomalous self-energy Σ^{ano} . Here, we adopt the recently developed maximum entropy analytic continuation method for Σ^{ano} [45]. In this approach one defines an auxiliary self-energy with positive-definite spectral weight to compute

the real-frequency Σ^{ano} . We calculate the optical conductivity $\sigma_1(\omega)$ within the framework of linear response and in the long-wave-length limit [46, 47]. In the superconducting state, one has to express the dipole matrix elements and matrix spectral function [48] in the Nambu formalism.

We first consider the temperature dependence of $A(\mathbf{k}, \omega)$ and $\sigma_1(\omega)$ at fixed volume. Here, we choose the volume $V = 750 \text{ \AA}^3$ corresponding to moderate correlations ($U_{\text{eff}}/W \approx 1.74$) and $T_c = 33.7$ K located slightly to the left of the maximum of the SC dome. The results are shown in Fig. 3. At high temperature, $T = 200$ K, the system is not very coherent, as shown in panel (d). The bandwidth is renormalized with respect to the non-interacting W by about a factor of three, consistent with the mass enhancement $m^*/m \approx 1 - \text{Im}\Sigma^{\text{nor}}(i\omega_0)/\omega_0 = 3.3$, where $\omega_0 = \pi T$ is the first Matsubara frequency. Close to, but above T_c , the quasi-particle bands become sharper, as shown in panel (c). When the temperature drops below T_c , a superconducting gap opens at all momenta. At $T = 10$ K ($< T_c/3$, panel (b)), one observes a gap of 4.6 meV (estimated from the \mathbf{k} -integrated normal spectra, see inset) and back-bending of the Bogolyubov quasi-particle bands.

The temperature dependence of the real part of the conductivity, $\sigma_1(\omega)$, is shown in panel (a). As one decreases T from 100 K (black line in panel (a)) to 50 K

(orange line), the Drude peak of $\sigma_1(\omega)$ grows in height but narrows, which results in a loss of spectral weight in the energy range from 5 meV to 50 meV. At $T = 30$ K (blue line), the system enters the SC phase, marked by additional spectral weight loss below 30 meV, while a narrow Drude feature still persists. As one decreases T further from $T = 15$ K (green) to 10 K (red), the Drude peak becomes very small and sharp. The persistent Drude peak at $T = 10$ K in a very low-energy range ($\omega < 5$ meV) is related to the faint spectral weight in $A(\mathbf{k}, \omega)$ at the Fermi energy, which we have also previously observed in simulations of K_3C_{60} [45]. This faint spectral weight indicates the break-up of some Cooper pairs at nonzero temperature. The calculated $\sigma_1(\omega)$ is qualitatively consistent with the conductivity measurements for K_3C_{60} and Rb_3C_{60} [49].

Figure 4 shows the normal state ($T = 50$ K $> T_c$) $A(\mathbf{k}, \omega)$ (panels (b-d)) and $\sigma_1(\omega)$ (panel (a)) at different volumes. The first observation is that there is no Drude peak in $\sigma_1(\omega)$ for $V = 775 \text{ \AA}^3$ (green line), since at this volume the system is a Mott insulator with a fully gapped spectral function (panel (d)) above T_c . (This system is in the strong coupling regime with $U_{\text{eff}}/W \approx 2.35$.) The broad hump located around $\omega \sim 0.8$ eV arises from transitions between the Hubbard bands located at $\omega \sim \pm U_{\text{eff}}/2$ (panel (d), $U_{\text{eff}} \approx 0.86$ eV) and from transitions between the quasi-particle bands and the Hubbard bands [50]. As one decreases the volume by increasing pressure, a Mott insulator to metal transition is triggered and the system becomes more metallic, as seen from panels (c) ($V = 750 \text{ \AA}^3$) and (b) ($V = 724.8 \text{ \AA}^3$). The weight of the Hubbard bands is reduced and the width of the quasi-particle bands increases, as can be seen by comparing panels (b) and (c). As a result of this increasing bandwidth, the peak of $\sigma_1(\omega)$ in the energy range $0.06 < \omega < 0.3$ eV broadens and shifts to larger energies.

Discussion and Conclusions. We pointed out that the recently proposed $\text{Pa}\bar{3}$ structure of Cs_3C_{60} has an unrealistic spacing between the C_{60} molecules and Cs dopants and is structurally very unstable according to DFT calculations. Even if the $\text{Pa}\bar{3}$ structure could be somehow realized at ambient pressure, this system would feature

a large crystal field splitting between the t_{1u} bands, and thus most likely not exhibit superconductivity.

Since the $\text{Pa}\bar{3}$ structure relaxes to the stable FCC structure in DFT, we studied the electronic properties of the FCC structure using state-of-the-art DFT+DMFT simulations in the Nambu-formalism. The superconducting order parameter, critical temperature T_c , as well as the momentum-resolved spectra and optical conductivity in the SC phase and normal phase were calculated. Our calculated T_c values as a function of volume are consistent with previous experiments on the FCC structure. The transition between the s -wave SC phase and the Mott insulator at large volumes is found to be first order. The optical conductivity features a small Drude peak at the lowest temperature $T = 10$ K that we can reach, which is also consistent with optical measurements. This peak can be related to the faint spectral weight at the Fermi energy and the coexistence of paired and unpaired electrons in this small-gap superconductor.

Our study does not rule out the possibility of superconductivity in other fullerides with $\text{Pa}\bar{3}$ structure, such as $\text{Na}_2\text{Rb}_x\text{Cs}_{1-x}\text{C}_{60}$ [17, 39]. We confirmed that $\text{Na}_2\text{CsC}_{60}$ is stable according to the DFT relaxation. It would be interesting to study the effect of the orientation of the C_{60} molecules on T_c . Since the symmetry is lowered compared to the FCC structure, the resulting crystal field splitting is expected to suppress local orbital fluctuations and lower T_c , compared to the FCC structure with the same volume.

Acknowledgements. — The DMFT calculations were performed on the Beo05 and Beo06 cluster at the University of Fribourg, using a code based on iQIST [51, 52]. C.Y. and P.W. acknowledge support from SNSF Grant No. 200021-196966. Y.N. acknowledge support from Grant-in-Aids for Scientific Research (JSPS KAKENHI) [Grant Nos. JP23H04869, JP23H04519, JP23K03307, and JP21H01041], MEXT as “Program for Promoting Researches on the Supercomputer Fugaku” (Grant No. JPMXP1020230411), and JST (Grant No. JPMJPF2221). KP acknowledges financial support by Grants-in-Aid for Scientific Research (JSPS KAKENHI Grant Numbers JP21H01907 and JP22K18693).

-
- [1] O. Gunnarsson, Rev. Mod. Phys. **69**, 575 (1997).
 - [2] Massimo Capone, Michele Fabrizio, Claudio Castellani, and Erio Tosatti, Rev. Mod. Phys. **81**, 943 (2009).
 - [3] Palstra, T. T. M., O. Zhou, Y. Iwasa, P. E. Sulewski, R. M. Fleming, and B. R. Zegarski. Solid State Commun. **93**, 327 (1995).
 - [4] A. Y. Ganin, Y. Takabayashi, Y. Z. Khimyak, S. Margadonna, A. Tamai, M. J. Rosseinsky, K. Prassides. Nat. Mater. **7**, 367 (2008).
 - [5] Y. Takabayashi, A. Y. Ganin, P. Jeglič, D. Arçon, T. Takano, Y. Iwasa, Y. Ohishi, M. Takata, N. Takeshita, K. Prassides, M. J. Rosseinsky. Science **323**, 1585 (2009)
 - [6] R. H. Zadik, Y. Takabayashi, G. Klupp, *et al.*, Sci. Adv. **1**, e1500059 (2015).
 - [7] J. E. Han, O. Gunnarsson, and V. H. Crespi, Phys. Rev. Lett. **90**, 167006 (2003).
 - [8] M. Capone, M. Fabrizio, C. Castellani, and E. Tosatti, Science **296**, 2364 (2002).
 - [9] Y. Nomura, K. Nakamura, and R. Arita, Phys. Rev. B **85**, 155452 (2012).
 - [10] Y. Nomura, S. Sakai, M. Capone, and R. Arita, Sci. Adv. **1**, e1500568 (2015).
 - [11] S. Hoshino, and P. Werner, Phys. Rev. Lett. **118**, 177002 (2017).
 - [12] C. Yue, S. Hoshino, and P. Werner, Phys. Rev. B **102**, 195103 (2020).
 - [13] S. Hoshino, and P. Werner, Phys. Rev. Lett. **115**, 247001 (2015).

- [14] P. Werner, S. Hoshino, and H. Shinaoka, *Phys. Rev. B* **94**, 245134 (2016).
- [15] D. Peng, R.-S. Wang, L.-N. Zong, X.-J. Chen. *arXiv* **2208**, 09429 (2022).
- [16] O. Zhou, G. B. M. Vaughan, Q. Zhu, J.E. Fischer, P. A. Heinney, N. Coustel, John P. McCauley, Jr., and A. B. Smith III, *Science* **255**, 833 (1992).
- [17] K. Prassides, C. Christides, I. M. Thomas, J. Mizuki, K. Tanigaki, I. Hirose, T. W. Ebbesen *Science* **263**, 960 (1994).
- [18] P. A. Heiney, J. E. Fisher, A. R. McGhie, W. J. Romanow, A. M. Denenstein, J. P. McCauley Jr., A. B. Smith, and D. E. Cox. *Phys. Rev. Lett.* **66**, 2911 (1991)
- [19] Experimentally, the known fulleride compounds show orientational or merohedral disorder. Such type of disorder is not considered in our calculations.
- [20] G. Kresse, and J. Hafner, *Phys. Rev. B* **47**, 558 (1993).
- [21] G. Kresse, and J. Furthmüller, *Comput. Mater. Sci.* **6**, 15 (1996).
- [22] A. Y. Ganin, Y. Takabayashi, P. Jeglic, D. Arcon, A. Potocnik, P. J. Baker, Y. Ohishi, M. T. McDonald, M. D. Tzirakis, A. McLennan, G. R. Darling, M. Takata, M. J. Rosseinsky, and K. Prassides, *Nature* **466**, 221 (2010).
- [23] G. Kresse, and J. Furthmüller, *Phys. Rev. B* **54**, 11169 (1996).
- [24] A. A. Mostofi, J. R. Yates, G. Pizzi, Y.-S. Lee, I. Souza, D. Vanderbilt, and N. Marzari, *Comput. Phys. Commun.* **185**, 2309 (2014).
- [25] G. Pizzi, V. Vitale, R. Arita *et al.*, *J. Phys.: Condens. Matter* **32**, 165902 (2020).
- [26] M. Kim, Y. Nomura, M. Ferrero, P. Seth, O. Parcollet, and A. Georges, *Phys. Rev. B* **94**, 155152 (2016).
- [27] C. Yue, Y. Nomura, and P. Werner, *Phys. Rev. Lett.* **129**, 066403 (2022).
- [28] C. Yue, S. Hoshino, A. Koga, and P. Werner, *Phys. Rev. B* **104**, 075107 (2021).
- [29] F. Aryasetiawan, M. Imada, A. Georges, G. Kotliar, S. Biermann, and A. I. Lichtenstein. *Phys. Rev. B* **70**, 195104 (2004)
- [30] Y. Nomura, and R. Arita, *Phys. Rev. B* **92**, 245108 (2015).
- [31] A. Georges, G. Kotliar, W. Krauth, and M. J. Rozenberg, *Rev. Mod. Phys.* **68**, 13 (1996).
- [32] G. Kotliar, S. Y. Savrasov, K. Haule, V. S. Oudovenko, O. Parcollet, and C. A. Marianetti, *Rev. Mod. Phys.* **78**, 86 (2006).
- [33] P. Werner, A. Comanac, L. de' Medici, M. Troyer, and A. J. Millis, *Phys. Rev. Lett.* **97**, 076405 (2006).
- [34] E. Gull, A. J. Millis, A. I. Lichtenstein, A. N. Rubtsov, M. Troyer, and P. Werner, *Rev. Mod. Phys.* **83**, 349 (2011).
- [35] P. Sémon, G. Sordi, and A.-M. S. Tremblay, *Phys. Rev. B* **89**, 165113 (2014).
- [36] P. Gunacker, M. Wallerberger, E. Gull, A. Hausoel, G. Sangiovanni, and K. Held, *Phys. Rev. B* **92**, 155102 (2015).
- [37] C. Yue, H. Aoki, and P. Werner, *Phys. Rev. B* **106**, L180506 (2022).
- [38] A. Hausoel, M. Wallerberger, J. Kaufmann, K. Held and G. Sangiovanni. *arXiv:2211.06266* (2022).
- [39] T. Yildirim, J. E. Fischer, R. Dinnebier, P. W. Stephens, and C. L. Lin, *Solid State Commun.* **93**, 269 (1995).
- [40] C. M. Brown, T. Takenobu, K. Kordatos, K. Prassides, Y. Iwasa, K. Tanigaki, *Phys. Rev. B* **59**, 4439 (1999).
- [41] Nagamatsu, J., Nakagawa, N., Muranaka, T., Zenitani, Y. Akimitsu, J. Superconductivity at 39 K in magnesium diboride. *Nature* **410**, 63 (2001).
- [42] Hebard, A. F., Rosseinsky, M. J., Haddon, R. C., Murphy, D. W., Glarum, S. H., Palstra, T. T. M., Ramirez, A. P. and Kortan, A. R. *Nature* **350**, 600 (1991).
- [43] S. Lefebvre, P. Wzietek, S. Brown, C. Bourbonnais, D. Jerome, C. Meziere, M. Fourmigue, and P. Batail, *Phys. Rev. Lett.* **85**, 5420 (2000).
- [44] G. Sordi, P. Sémon, K. Haule, and A.-M. S. Tremblay, *Phys. Rev. Lett.* **108**, 216401 (2012).
- [45] C. Yue and P. Werner, *arXiv:2203.16888* (2023).
- [46] J.M. Tomczak and S. Biermann, *Phys. Rev. B* **80**, 085117 (2009).
- [47] P. Wissgott, J. Kuneš, A. Toschi and K. Held, *Phys. Rev. B* **85**, 205133 (2012).
- [48] E. Assmann, P. Wissgott, J. Kuneš, A. Toschi, P. Blaha, K. Held, *Comput. Phys. Commun.* **202**, 1 (2016).
- [49] L. Degiorgi, G. Briceno, M. S. Fuhrer, A. Zettl, and P. Wachter, *Nature* **369**, 541-543 (1994).
- [50] Note that only the t_{1u} orbitals are included in our DMFT simulations. In experiments, excitations to other bands could also occur at these energies.
- [51] L. Huang, Y. Wang, Z. Y. Meng, L. Du, P. Werner, and X. Dai, *Comput. Phys. Commun* **195**, 140 (2015).
- [52] L. Huang, *Comput. Phys. Commun* **221**, 423 (2017).

Supplementary Information

Instability of $\text{Pa}\bar{3} \text{Cs}_3\text{C}_{60}$ at ambient pressure and superconducting state of the FCC phase

Changming Yue,^{1,*} Yusuke Nomura,² Kosmas Prassides,³ and Philipp Werner^{1,†}

¹*Department of Physics, University of Fribourg, 1700 Fribourg, Switzerland*

²*Department of Applied Physics and Physico-Informatics, Keio University, 3-14-1 Hiyoshi, Kohoku-ku, Yokohama, 223-8522, Japan*

³*Department of Physics, Graduate School of Science, Osaka Metropolitan University, Osaka 599-8531, Japan*

SM1. SMALLEST DISTANCE BETWEEN TETRAHEDRAL Cs AND C IN $\text{Pa}\bar{3} \text{Cs}_3\text{C}_{60}$

Figure S1 shows the coordination environment of tetrahedral Cs (red dot) in $\text{Pa}\bar{3} \text{Cs}_3\text{C}_{60}$ reported in Ref. 1. The smallest distances between the nearest carbon atom and the tetrahedral Cs are shown by three equivalent “bonds” connecting this Cs and three nearby C_{60} molecules colored in gold, green and blue, respectively. The distance is 2.70 Å, which is significantly smaller than the sum of the ionic radius of Cs^+ ($r_{\text{Cs}^+} = 1.67$ Å) and the van der Waals radius of C ($r_{\text{vdW,C}} = 1.7$ Å). For this reason, it is unlikely that this structure is stable at ambient pressure.

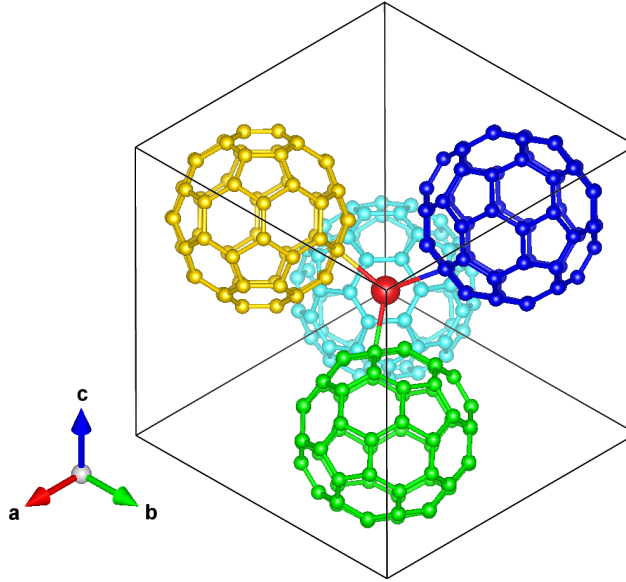


FIG. S1. The coordination environment of tetrahedral Cs in $\text{Pa}\bar{3} \text{Cs}_3\text{C}_{60}$ viewed along the C_3 symmetric axis $[\bar{1}\bar{1}\bar{1}]$. For a better visualization, we use different colors to distinguish the C_{60} molecules with different orientations (as in the main text).

* changming.yue@unifr.ch

† philipp.werner@unifr.ch

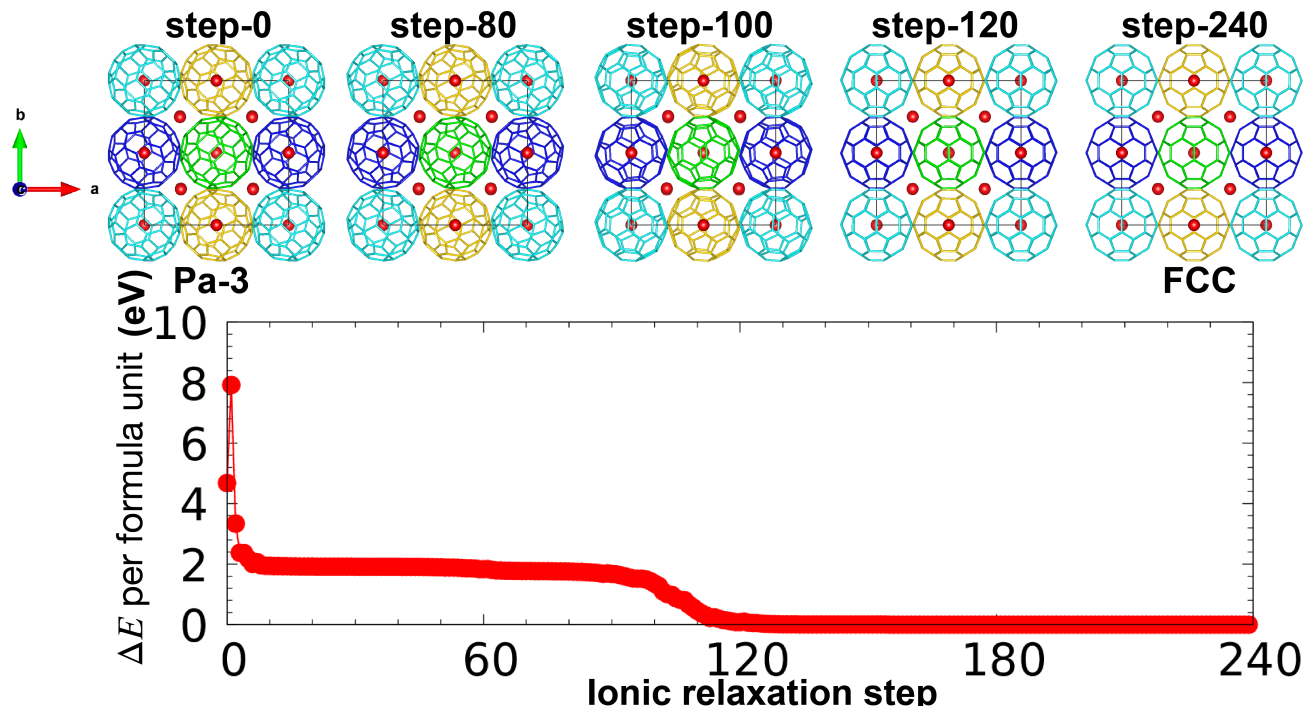


FIG. S2. Top panel: Evolution of the structure of Cs_3C_{60} during the relaxation starting from the space group $\text{Pa}\bar{3}$. Lower panel (same as Fig. 2(i) in the main text): Energy difference ΔE per formula unit between the structure under relaxation and the final stable FCC structure as a function of ionic relaxation steps.

SM2. STRUCTURAL RELAXATION

The density functional theory (DFT) calculations, including the structural relaxation and band structure calculations, are performed using the Vienna ab initio simulation package (VASP) code with the Perdew-Burke-Ernzerhof exchange-correlation functional [2–4] and the cutoff energy 500 eV. We sample the Brillouin zone using $7 \times 7 \times 7$ mesh grids for the DFT calculations and $5 \times 5 \times 5$ mesh grids for the constrained random phase approximation calculation.

The structural relaxation is performed with fixed volume. Figure S2 shows how the structure of Cs_3C_{60} evolves during the relaxation starting from the $\text{Pa}\bar{3}$ structure reported in Ref. 1. As we can see from the top panel, the C_{60} molecules are rotated during the relaxation, especially between step 80 and step 120. In the relaxed structure, there is no difference in the orientations of the C_{60} molecules and the system corresponds to the space group $\text{Fm}\bar{3}$ (FCC).

SM3. $\text{Na}_2\text{CsC}_{60}$

$\text{Na}_2\text{CsC}_{60}$ crystallizes in the space group $\text{Pa}\bar{3}$. We relax this system starting from the main orientation of the structure reported in Ref. [5]. As shown by the lower panel of Fig. S3, the energy gain after relaxation is 0.6 eV per formula unit, which is much smaller than in the case of $\text{Pa}\bar{3}$ Cs_3C_{60} after relaxation (4.67 eV). Furthermore, the structure is only changed slightly during the relaxation and the space group remains $\text{Pa}\bar{3}$. Hence, $\text{Pa}\bar{3}$ $\text{Na}_2\text{CsC}_{60}$ reported in Ref. [5] is a stable structure, in contrast to $\text{Pa}\bar{3}$ Cs_3C_{60} reported in Ref. [1].

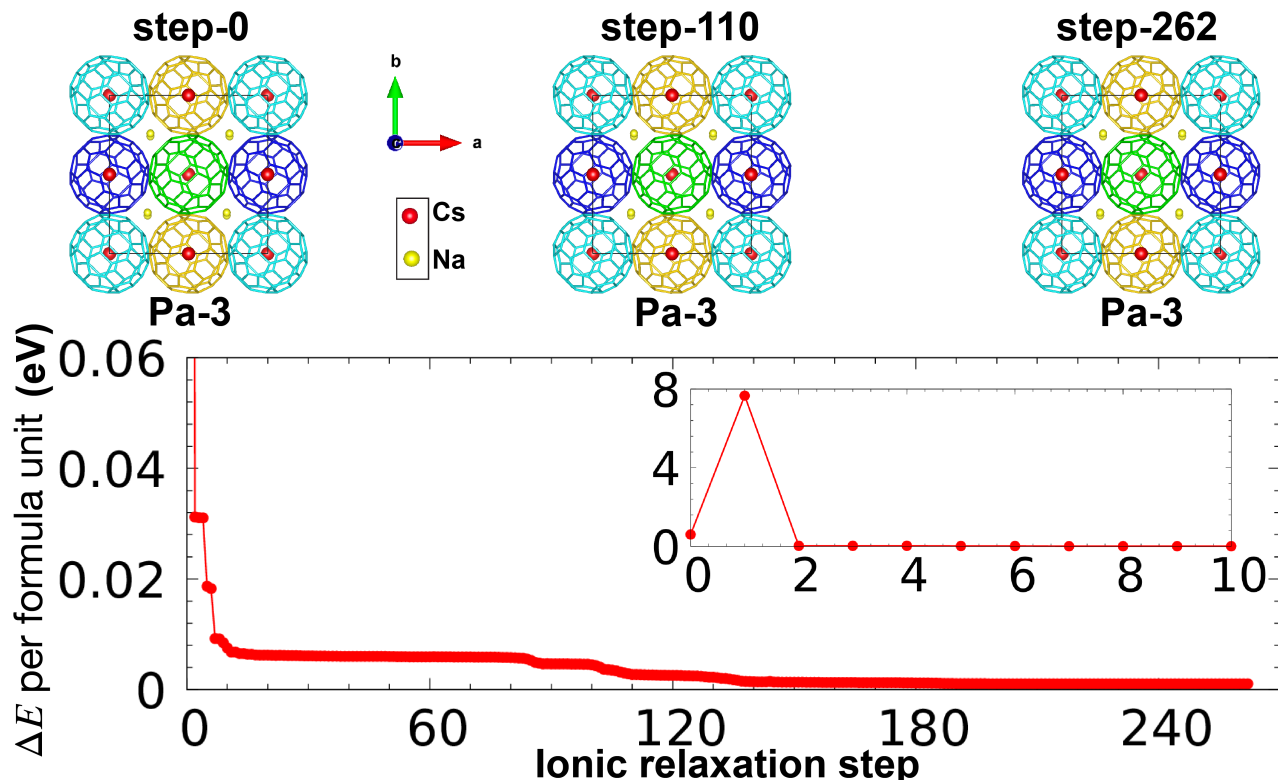


FIG. S3. Top panel: Evolution of the structure of $\text{Na}_2\text{CsC}_{60}$ during relaxation starting from the space group $\text{Pa}\bar{3}$. Lower panel: Energy difference ΔE per formula unit between the structure under relaxation and the final stable structure as a function of ionic relaxation steps. The inset shows ΔE for the first 11 steps on a larger y -range.

-
- [1] D. Peng, R.-S. Wang, L.-N. Zong, X.-J. Chen. arXiv **2208**, 09429 (2022).
 - [2] G. Kresse, and J. Hafner, Phys. Rev. B **47**, 558 (1993).
 - [3] G. Kresse, and J. Furthmüller, Comput. Mater. Sci. **6**, 15 (1996).
 - [4] G. Kresse, and J. Furthmüller, Phys. Rev. B **54**, 11169 (1996).
 - [5] K. Prassides, C. Christides, I. M. Thomas, J. Mizuki, K. Tanigaki, I. Hirose, T. W. Ebbesen, Science **263**, 950 (1994).